Supplement of Eur. J. Mineral., 38, 249–262, 2026
https://doi.org/10.5194/ejm-38-249-2026-supplement

European Journal of Mineralogy
Open Access

Supplement of

The Tibet leucogranite as a potential high-purity-quartz raw material: first discovery and case study from the Dinggye area

Liting Sun et al.

Correspondence to: Xiaoyong Yang (xyyang@ustc.edu.cn) and Mei Xia (xm851102@ustc.edu.cn)

Sect. S1 Analytical Methods

Sect. S1.1 Quartz purification experiment and flow chart

Building upon established HPQ extraction and purification workflows (Xia et al., 2024; Shao et al., 2026), this study adapted these techniques for leucogranite-hosted quartz (the specific process is shown in Fig. S1).

Firstly, a jaw crusher was used to crush the raw quartz ores XZ-BG and XZ-WJ, and quartz sand with particle sizes between 40 and 200 mesh was sieved and reserved (Xie et al., 2024). During the crushing process, mechanically introduced iron may be carried with the quartz sand; therefore, strong magnets were applied for preliminary magnetic separation (Liu et al., 2023; Xie et al., 2024). Secondly, the pre-treated quartz sand underwent ultrasonic washing and desliming prior to flotation (Xia et al., 2024): washing for 30 minutes under a pulp concentration of 50%, with water changed every 10 minutes, followed by drying.

Flotation was conducted using ultrapure water, with the temperature maintained at 50-60°C and pH adjusted to ~2.5 using hydrofluoric acid (HF), consistent with HF-assisted quartz/silicate flotation practice (Wang et al., 2018). After conditioning for 2 minutes, 2 mL dodecylamine (DDA) collector and 2 mL sodium dodecylbenzenesulfonate (SDBS) frother were added, and the air flow rate was set to 0.25 m^3/h. The floated quartz sand was calcined in a muffle furnace at 1050°C for 1 hour, followed by acid leaching (Shao et al., 2026). Specifically, 10 g quartz sand was reacted in a polytetrafluoroethylene reactor with 10 mL mixed acid (HCl: HF: HNO_3 = 3:1:1) at 90°C for 24 h, then ultrasonically rinsed with ultrapure water to neutral pH to remove residual acid; calcination and acid leaching were repeated to enhance impurity removal (Ge et al., 2025).

Finally, chlorination roasting was performed to further remove volatile metal chlorides. The acid-leached quartz sand was placed in a heatable quartz glass tube, and Cl_2 gas was continuously introduced at 1050°C for 2 h, followed by Ar purging to remove residual Cl_2 (Guo et al., 2024). After cooling, the purified quartz sand was collected as the final high-purity product.

.

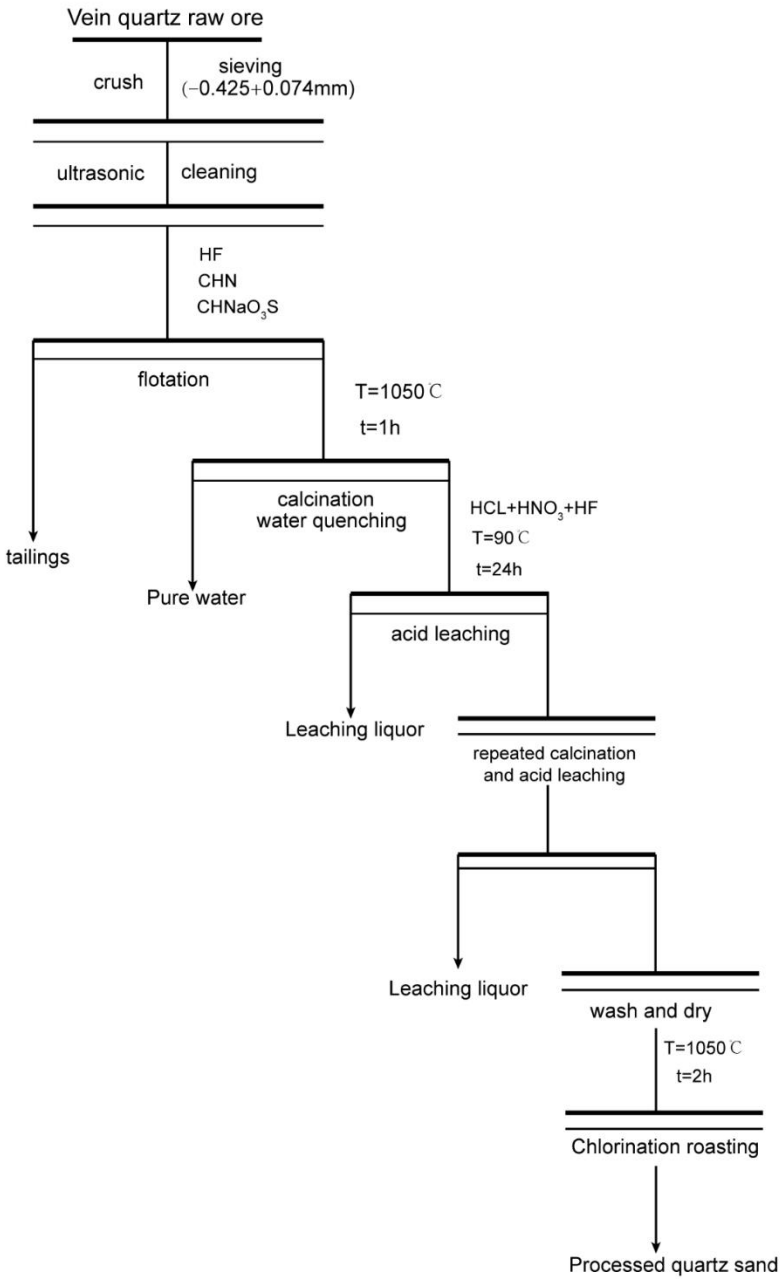

Figure S1. Quartz purification experiment flow chart.

Sect. S1.2 Microscope observation

Prepare 100μm probe sections from leucogranite samples, and the petrological characteristics of the sample were observed by transmission polarization microscope (TPM, Nikon DS-RI2, Tokyo, Japan) such as structure, fracture development, mineral composition, and particle size.

Sect. S1.3 Major element XRF mapping

The composition, microstructure characteristics of the minerals in leucogranites

were determined by qualitative major element XRF mapping of bulk thin sections using the high-resolution μ-XRF (XRF) M4 Tornado spectrometer equipped by the Key Laboratory of Crust and Mantle Matter and Environment, University of Science and Technology of China, Hefei. The operating conditions are a counting time of 30ms, an acceleration voltage of 50 kV, a probe current of 200 μA, and the spatial resolution in the x and y directions is 25 μm. The μ-XRF diagram was processed by ARMICS software, and the modal proportions of the ore phase were obtained.

Sect. S1.4 X-ray fluorescence spectrometer (XRF) analysis

The examination of major elements for the whole rock study was done by wavelength dispersive X-ray fluorescence spectrometer (XRF) at the Key Laboratory of Crust-Mantle Material and Environment, University of Science and Technology of China, Hefei. The major elements in the entire rock are melted using lithium metaborate as a melting aid. Firstly, accurately weigh 0.6g of whole rock powder (200 mesh) and place it in a known-weight ceramic crucible. Burn it in a muffle furnace at 920°C until the weight remains constant. After the sample is burned, cool it to room temperature. Precisely measure the mass of the sample and crucible post-combustion. To ascertain the loss on ignition (LOI) of the sample, the essential measurement involves calculating the variance in weight between the sample and the crucible before and after the burning process. Subsequently, the burned sample was mixed with 6g of lithium borate flux ($Li_2B_4O_7$: $LiBO_2$: LiF=9:2:1) and fully melted and homogenized at a high temperature of 1050°C. The molten material was poured out to make a flat glass plate for analysis. The analysis process involves monitoring data quality through a series of standard and duplicate samples. Long-term data monitoring indicates that the uncertainty of principal element analysis is better than ± 5%.

Sect. S1.5 Analysis of chemical composition in situ of quartz by LA-ICP-MS

The concentrations of trace elements in the quartz samples were measured through the technique of laser ablation inductively coupled plasma mass spectrometry (LA-ICP-MS). This process was conducted using an Agilent 7900 Quadrupole ICP-MS and a Photon Machines Analyte HE 193-nm ArF Excimer laser ablation system at the Mineral

Geochemistry Lab within the Ore Deposit and Exploration Center at Hefei University of Technology, China. Helium was used as the carrier gas along with argon through a T-connector to ensure stable and optimal excitation conditions before entering the ICP-MS equipment.

The methodology adopted a single-spot ablation approach using a laser spot diameter of 30 μm, operating at a frequency of 7 Hz, with an energy density of around 7 J/cm^2. Each analysis cycle comprised a 20-second background acquisition (gas blank) and a 40-second data acquisition from the sample. NIST610 and NIST612 were standard reference materials to execute quality control procedures and set detection limits with BCR-2G to plot the curve and calibrate the results. Ten sets of unknown sample sets were conducted using the reference materials both before and after each set of spots.

The analysis of offline data was carried out using Spotanalysis1.0. Without comparing the silicate minerals' trace element compositions to those of other reference materials, they were calibrated independently. To represent 100 % m/m for a particular anhydrous silicate material, the total element concentrations underwent standardization and were represented as oxides based on the oxidation states of the constituent elements inside the silicate.

Sect. S1.6 Bulk chemical composition analysis by ICP-MS

The impurity trace elements in the purified quartz sand were determined using the Agilent 7700e quadrupole ICP-MS from the Inductively Coupled Plasma Mass Spectrometry (ICP-MS) Laboratory at the University of Science and Technology of China, Hefei. Weigh approximately 50 mg of the sample and GBW07837 quartz reference material and dissolve it in purified hydrofluoric acid (HF) and nitric acid (HNO_3) to a volume of 20 ml.

The treated sample solution was analyzed on an Agilent 7700 ICP-MS. The RF power is 1350 W and the atomized gas flow rate is 1.0 L/min. In order to eliminate the interference of polyatomic ionic impurities, 3.5 ml/min of helium was introduced as a collision gas during the test. The standard calibration curve solution used to calculate the content of the sample solution was NCS181036 using a 13-element mixed standard solution prepared with Beijing NCS Detection Technology Co., Ltd.

Sect. S1.7 Titanium-in-quartz thermometer analysis

The quartz-titanium thermometer is a geological thermometer used to estimate geological temperatures based on the titanium content in quartz. Its calculation involves several empirical formulas, which are based on experimental data and theoretical models. In the pale-colored granite of the Rimana dome, no diagnostic minerals such as sphene, rutile, or magnetite-ilmenite were found. Therefore, this study adopts the temperature calculation formula for systems without rutile, as proposed by Hayden and Watson (2007):

$$T(°C)= -3765/[\mathrm{Log}(X_{Ti}^{Qtz} /a_{TiO2})-5.69]-273 \cdots\cdots\cdots\cdots\cdots\cdots (Eq.S1)$$

In (Eq.S1), X_{T}^{Qtz} represents the mass concentration of Ti in quartz, expressed in ppm; $aTiO_2$ refers to the Ti activity in the system. Hayden (2007) indicated that in the absence of diagnostic minerals in the system, the TiO_2 activity is assumed to be around 0.5-0.6.

When using the quartz-titanium thermometer for calculations, this study assumes $aTiO_2$ values of 0.5, 0.55, and 0.6, and finds that the results are similar (±13°C). Therefore, the temperature calculated using the middle value of Ti activity, 0.55, is taken as the final result.

Sect. S2 The comparison chart of the major element data of ADM leucogranite and the Himalayan leucogranite from the literature.

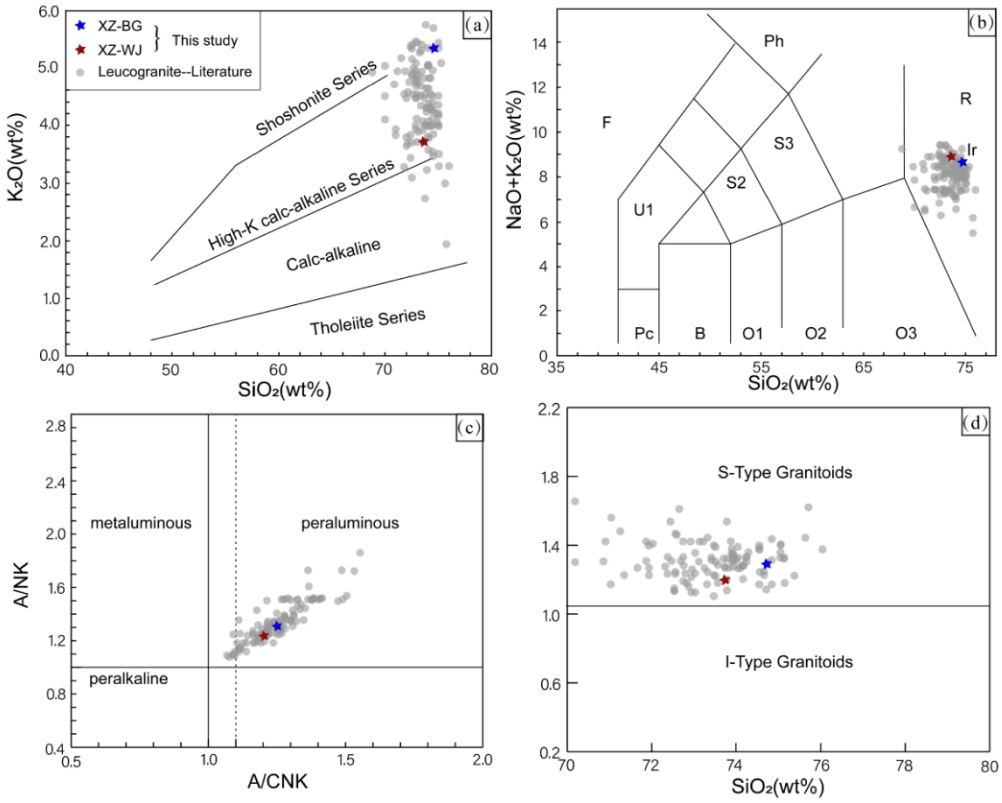

Figure S2. Classification diagrams. (a) K_2O versus SiO_2 diagram for the leucogranite （after Peccerillo and Taylor, 1976）;(b) Rock suite classification in the plot of (Na_2O + K_2O) versus SiO_2 (after Middlemost,1994); F-Foidite, Pc-Picrobasalt, U1-Olivine, Ph-Phonolite, B-Gabbro, S2-Monzodiorite, S3-Monzonite, O1-Gabbroic diorite, O2-Diorite, O3-Granodiorite, R-Granite; (c) A/CNK versus A/NK diagram (after Maniar and Piccoli, 1989); (d) alumina index diagram for leucogranite. Boundary between I-type and S-type according to Chappell and White, 1992).

*The dataset comprises geochemical and/or petrological data from S-type peraluminous leucogranites, collected from several domes, metamorphic core complexes, and key plutons within the Himalayan belt (including the Tethyan Himalayan segment). Representative examples include the Gurla Mandhata, Malashan–Paiku, Xiaru, and Shisha Pangma massifs. The data are sourced from the following studies: Cheng et al., 2020; Gao et al., 2013, Gao et al., 2016; Gou et al., 2016; Guo and Wilson. 2012; Hu et al., 2017; Huang et al., 2017; Liu et al., 2016; Scaillet et al., 1990; Searle et al., 1997; Visonà and Lombardo. 2002.

Sect. S3 Diagrams of Al-Li, Al-Ti, Al-Na, Al-K, Al-Ge, Ge-Ti of quartz in XZ-BG and XZ-WJ

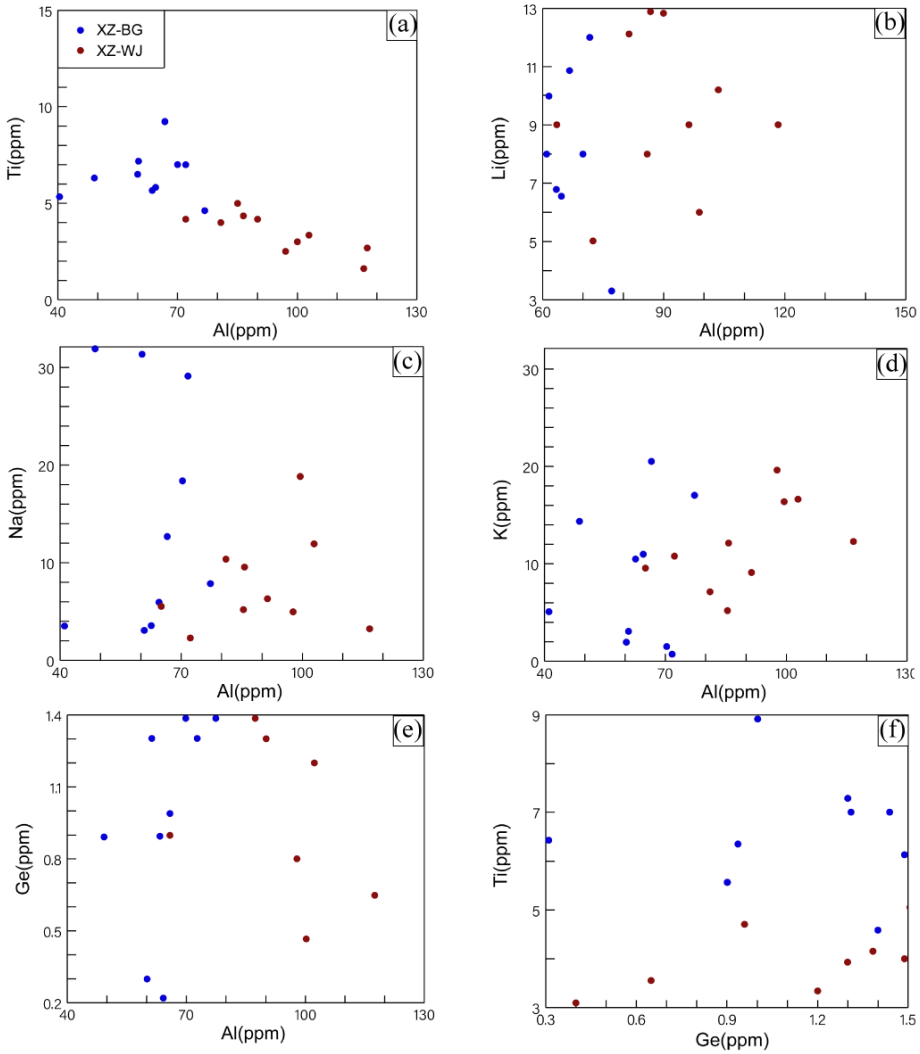

Figure S3. Diagrams of Al-Li, Al-Ti, Al-Na, Al-K, Al-Ge, Ge-Ti of quartz in XZ-BG and XZ-WJ.

References

Chappell, B.W., and White, A.J.R.: I- and S-type granites in the Lachlan Fold Belt, Earth Environ Sci Trans R Soc Edinb, 83, 1-26, https://doi.org/10.1017/S0263593300007720, 1992.

Cheng, L., Zhang, C., and Yang, X.: Petrogenesis of deformed tourmaline leucogranite in the Gurla Mandhata metamorphic core complex, Southwestern Tibet, Lithos, 364-365, 105533, https://doi.org/10.1016/j.lithos.2020.105533, 2020.

Ge, X., Ren, Z., Mu, J., Guo, Z., He, Y., and Song, Y.: Preparation of High Purity Quartz Sand by Mixed Acid Leaching from Quartz Associated with Kaolin and Its Leaching Kinetics Analysis, J. Wuhan Univ. Technol. Mater. Sci. Ed., 40, 1048-1056, https://doi.org/10.1007/s11595-025-3143-3, 2025.

Gao, L.E., Zeng, L.S., Gao, J.H., Shang, Z., Hou, K.J., and Wang, Q.: Oligocene crustal anatexis in the Tethyan Himalaya, southern Tibet, Lithos, 264, 201-209, https://doi.org/10.1016/j.lithos.2016.08.038, 2016.

Gao, L.E., Zeng, L.S., Hou, K.J., Guo, C.L., Tang, S.H., Xie, K.J., Hu, G.Y., and Wang, L.: Episodic crustal anatexis and the formation of Paiku composite leucogranitic pluton in the Malashan Gneiss Dome, Southern Tibet, Chin. Sci. Bull., 58, 3546-3563, https://doi.org/10.1007/s11434-013-5792-4, 2013.

Gou, Z., Zhang, Z., Dong, X., Xiang, H., Ding, H., Tian, Z., and Lei, H.: Petrogenesis and tectonic implications of the Yadong leucogranites, southern Himalaya, Lithos, 256-257, 300-310, https://doi.org/10.1016/j.lithos.2016.04.009, 2016.

Guo, Z.F., and Wilson, M.: The Himalayan leucogranites: Constraints on the nature of their crustal source region and geodynamic setting, Gondwana Res., 22, 360-376, https://doi.org/10.1016/j.gr.2011.07.027, 2012.

Guo, W., Lu, H., Zhang, Z., Jiang, L., Wu, H., Liu, D., and Chi, R.: Crystal structure transformation and lattice impurities migration of quartz during chlorine roasting, Int. J. Min. Sci. Technol., 34, 1465-1474, https://doi.org/10.1016/j.ijmst.2024.09.004, 2024.

Hayden, L.A., and Watson, E.B.: Rutile saturation in hydrous siliceous melts and its bearing on Ti-thermometry of quartz and zircon, Earth Planet. Sci. Lett., 258, 561-568, https://doi.org/10.1016/j.epsl.2007.04.020, 2007.

Hu, G.Y., Zeng, L.S., Gao, L.E., Chen, H., Liu, Q.P., and Guo, Y.S.: Anatexis of Paleoproterozoic rock units in the Gurla Mandhata dome, Himalayan orogen, Acta Petrol. Sin., 33, 3710-3728, 2017.

Huang, C.M., Zhao, Z.D., Li, G.M., Zhu, D.C., Liu, D., and Shi, Q.S.: Leucogranites in Lhozag, southern Tibet: Implications for the tectonic evolution of the eastern Himalaya, Lithos, 294-295, 246-262, https://doi.org/10.1016/j.lithos.2017.09.014, 2017.

Liu, C., Wang, W., Wang, H., Zhu, C., and Ren, B.: A review on removal of iron impurities from quartz mineral, Minerals, 13, 1128, https://doi.org/10.3390/min13091128, 2023.

Liu, Z.C., Wu, F.Y., Ding, L., Liu, X.C., Wang, J.G., and Ji, W.Q.: Highly fractionated La te Eocene (~35 Ma) leucogranite in the Xiaru Dome, Tethyan Himalaya, South Tibet, Li thos, 240-243, 337-354, https://doi.org/10.1016/j.lithos.2015.11.026, 2016.

Maniar, P.D., and Piccoli, P.M.: Tectonic discrimination of granitoids, GSA Bulletin, 101, 635-643, https://doi.org/10.1130/0016-7606(1989)101<0635:TDOG>2.3.CO;2, 1989.

Middlemost, E.A.K.: Naming materials in the magma/igneous rock system, Earth-Sci. Rev., 37, 215-224, https://doi.org/10.1016/0012-8252(94)90029-9, 1994.

Peacock, M.A.: Classification of igneous rock series, J. Geol., 39, 54-67, https://doi.org/10.1086/623788, 1931.

Scaillet, B., France-Lanord, C., and Le Fort, P.: Badrinath-Gangotri plutons (Garhwal, Indi a): petrological and geochemical evidence for fractionation processes in a high Himalaya n leucogranite, J. Volcanol. Geotherm. Res., 44, 163-188, https://doi.org/10.1016/0377-027 3(90)90017-A, 1990.

Searle, M.P., Parrish, R.R., Hodges, K.V., Hurford, A., Ayres, M.W., and Whitehouse, M.J.: Shisha Pangma leucogranite, south Tibetan Himalaya: Field relations, geochemistry, age, origin, and emplacement, J. Geol., 105, 295-318, https://doi.org/10.1086/515924, 1997.

Shao, H., Zhang, X., Li, W., Han, Y., and Li, Z.: Review of advanced purification technol ogies for high-purity quartz materials, Mater. Res. Bull., 196, 113904, https://doi.org/10.1 016/j.materresbull.2025.113904, 2026.

Visonà, D., and Lombardo, B.: Two-mica and tourmaline leucogranites from the Everest-M akalu region (Nepal-Tibet). Himalayan leucogranite genesis by isobaric heating?, Lithos, 62, 125-150, https://doi.org/10.1016/S0024-4937(02)00112-3, 2002.

Wang, W., Cong, J., Deng, J., Weng, X., Lin, Y., Huang, Y., and Peng, T.: Developing ef fective separation of feldspar and quartz while recycling tailwater by HF pretreatment, Minerals, 8, 149, https://doi.org/10.3390/min8040149, 2018.

Xia, M., Yang, X., and Hou, Z.: Preparation of High-Purity Quartz Sand by Vein Quartz Purification and Characteristics: A Case Study of Pakistan Vein Quartz, Minerals, 14, 72 7, https://doi.org/10.3390/min14070727, 2024.

Xie, Y., Xia, M., Yang, X., Khan, I., and Hou, Z.: Research on 4N8 High-Purity Quartz Purification Technology Prepared Using Vein Quartz from Pakistan, Minerals, 14, 1049, https://doi.org/10.3390/min14101049, 2024.